Available online at www.sciencedirect.com

SciVerse ScienceDirect

Ceramics International 38 (2012) 5527–5533

CERAMICS INTERNATIONAL

www.elsevier.com/locate/ceramint

Influence of additives on microstructure and property of microarc oxidized Mg–Si–O coatings

Y.K. Pan [a,b], C.Z. Chen [a,b,*], D.G. Wang [a,b], X. Yu [a,b], Z.Q. Lin [a,b]

[a] Key Laboratory for Liquid–Solid Structural Evolution & Processing of Materials, Ministry of Education, Shandong University, Shandong, Jinan 250061, People's Republic of China

[b] School of Materials Science and Engineering, Shandong, Jinan 250061, People's Republic of China

Received 24 December 2011; received in revised form 28 March 2012; accepted 28 March 2012
Available online 4 April 2012

Abstract

Ceramic coatings were fabricated on ZK60 magnesium alloy substrate by microarc oxidation (MAO) in Na_2SiO_3–KOH base electrolyte with four kinds of additives (i.e. KF, NH_4HF_2, $C_3H_8O_3$ and H_2O_2). The effects of these additives on microstructure and property of coatings were investigated. The surface morphology, phase composition and corrosion resistance of the ceramic coatings were analyzed by scanning electron microscopy (SEM), X-ray diffraction (XRD) and simulation body fluid (SBF) immersion test respectively. It is found that different additives can change the spark discharge phenomenon during microarc oxidation. It is proved that both potassium fluoride (KF) and ammonium bifluoride (NH_4HF_2) promote discharge and accelerate reaction while the introduce of glycerol ($C_3H_8O_3$) leads to the refining of sparks and reduction of thermal effects. Results also demonstrate that the introduce of hydrogen peroxide (H_2O_2) contributes to the increase of coating surface roughness and enlargement of surface micropore size. XRD results indicate that the ceramic coatings are mainly composed of Mg_2SiO_4, $MgSiO_3$ and SiO_2. The introduce of H_2O_2 hinders the reaction between SiO_2 and MgO and creates favorable conditions for the formation of the MgO phase. The ceramic coatings formed in base electrolyte containing 7 g/L NH_4HF_2 and 5 mL/L $C_3H_8O_3$ exhibit the highest corrosion resistance.

Keywords: C. Corrosion; Magnesium alloy; Ceramic coating; Microarc oxidation; Additives

1. Introduction

By virtue of a unique combination of low density, high specific strength and good electromagnetic shielding characteristics [1], magnesium alloys show promise for use in many industrial applications. However, they are restricted in practice by their poor corrosion resistance [2–5]. There are many coating technologies available for corrosion protection and surface hardening of Mg alloys, such as anodizing [6,7], chemical conversion [8], electroplating, thermal spraying [9], biomimetic approach [10] and electrochemical deposition [11,12]. However, with inevitable limitations, they are not adequate for use in harsh service conditions, so proper surface treatment which can produce a relatively thick, dense, hard and anti-corrosive coating is required to improve properties of Mg alloys.

Microarc oxidation, based on conversional anodic oxidation technology, is a new promising surface treatment method to form in situ-grown ceramic coatings directly on so-called value metals, such as magnesium, aluminum, titanium and their alloys in weak-alkaline electrolyte without chromates at the voltage of alternating current up to 1000 V, usually accompanied by sparking and intensive gas evolution phenomenon at the anode surface [13–17]. The method of MAO has a lot of advantages over other surface treatments, e.g. excellent adhesion between coating and substrate, low energy consumption, easy controlling for processing and ecology-friendly process and products [18–21].

The structure and property of microarc coatings depend on many factors, such as substrate materials, electrolyte compositions, electrical parameters and so on. It is found that the electrolyte compositions play a key role in the MAO process [22], and some additives, such as KF, NH_4HF_2, $C_3H_8O_3$ and H_2O_2, are favorable to the MAO process and promising for the

* Corresponding author at: Key Laboratory for Liquid–Solid Structural Evolution & Processing of Materials, Ministry of Education, Department of Materials Science, Shandong University, Jing Shi Road # 17923, Shandong, Jinan 250061, China. Tel.: +86 531 88395991; fax: +86 531 88393538.
E-mail address: czchen@sdu.edu.cn (C.Z. Chen).

0272-8842/$36.00
http://dx.doi.org/10.1016/j.ceramint.2012.03.068

formation of ceramic coatings with good properties. The influence of $C_3H_8O_3$ on the characteristics of MAO coatings on AZ91D magnesium alloy has been studied [23]. However, research with MAO process on ZK60 magnesium alloy with introduce of KF, NH_4HF_2, $C_3H_8O_3$ and H_2O_2 in the base electrolyte is seldom conducted.

In this paper, KF, NH_4HF_2, $C_3H_8O_3$ and H_2O_2 were added into the silicate electrolyte one by one. Ceramic MAO coating with different performance were formed on ZK60 magnesium alloy. The effects of these additives on discharge phenomenon, coating appearance, phase composition and corrosion resistance were evaluated and a modified additive formula was obtained.

2. Experimental

2.1. Samples and solutions

Rectangular specimens (with dimensions of 8 mm × 10 mm × 12 mm) made of wrought magnesium alloy ZK60 (Zn 6%, Zr 0.45%, Mg balance) were used as the substrate material in the present study. Prior to the oxidation treatment, the samples were mechanically polished with carborundum waterproof abrasive paper up to 1000 grit, degreased with acetone following by rinsing with distilled water, and then immersed in electrolyte for MAO treatment after dried in warm air.

The base electrolyte was prepared from sodium silicate solution (15 g/L) and potassium hydroxide (5 g/L) in distilled water. The MAO process was carried out in the base electrolyte with introduce of different additives. The detailed information about the additives is shown in Table 1. All solutions were made from analytical grade reagents and distilled water.

For the MAO treatment, the specimens were used as anode, while a stainless steel container was used as cathode. The applied positive voltage was 400 V. The pulse frequency was fixed at 600 Hz. The duration for the MAO treatment was 30 min. A modified cooling water circulating pump was used to circulate the electrolyte in stainless bath to keep the electrolyte temperature below 50 °C. Meanwhile, fresh electrolyte was added to the bath with a stead flow through a self-made funnel to keep the pH of the electrolyte at about 6.5–7.0. Coated samples were flushed with distilled water after the treatment and dried with a blower.

Table 1
Composition and concentration of additives in MAO electrolyte.

Sample code	KF (g/L)	NH_4HF_2 (g/L)	$C_3H_8O_3$ (mL/L)	H_2O_2 (mL/L)
A1	3			
A2	5			
A3	7			
A4		3		
A5		5		
A6		7		
A7		7	5	
A8		7	10	
A9		7	15	
A10		7	5	10
A11		7	5	15
A12		7	5	20

2.2. Test and equipment

X-ray diffractometer (XRD, Philips X'Pert, Holland) with Cu-Kα radiation was used to analyze the phase components of the coating at a scanning speed of 4° min^{-1}. Scanning electron microscope (SEM) was employed to characterize the surface morphology and cross-section microstructure of the coating. The thickness of the MAO coatings was measured with a MINITEST 600B FN2 microprocessor coating thickness gauge (Elektro-physik Koln). The final coating thickness value quoted was the average of ten replicate measurements. Scratch tests were carried out using a WS-2004 scratch tester. A maximum 25 N load was applied at a loading speed of 10 N/min and a table speed of 2 mm/min. The corrosion resistance was analyzed by simulation body fluid (SBF) immersion test.

2.3. Corrosion test

The coatings prepared in this research would be served as materials of biomedical implants. So SBF immersion test was employed to evaluate the corrosion resistance. The treated samples were immersed in 1.0SBF with ion concentrations almost equal to those in human blood plasma [24]. The 1.0SBF was prepared by dissolving the reagents of NaCl, $NaHCO_3$, KCl, $K_2HPO_4{\cdot}3H_2O$, $MgCl_2{\cdot}6H_2O$, 1.0 mol/L HCl, $CaCl_2$, and Na_2SO_4 in distilled water at 36.5 ± 0.5 °C one by one in the above order. Then adjusted pH and buffered at pH 7.4 with trishydroxymethyl-aminomethane ($(CH_2OH)_3CNH_2$) and hydrochloric acid at 36.5 °C [25]. The solutions were freshed every 24 h and were kept colorless and stable without deposit during immersion for up to 9 d. Each sample was soaked in 60 mL of SBF in a plastic vial and placed in an oven at 36.5 °C. The mass of the samples was measured with electronic analytical balance with high precision. After immersing for 3, 5, 7and 9 d, the samples were removed from the SBF, washed with distilled water for 5 min, air-dried and weighed again, respectively.

3. Results and analysis

3.1. Phenomenon of MAO process

It was observed that the discharge spark color was different with introduce of different additives in base electrolyte during MAO process. The variation of the spark color represents reaction energy change, and the energy of white spark is much higher than that of orange one. The higher the energy is released, the denser the coating is formed. When KF alone was added into the base electrolyte, the discharge sparks were white and well distributed all over the sample surface. When NH_4HF_2 alone was added into the base electrolyte, the discharge sparks were still white, but they dispersed much more homogenously. The appearance of the coating formed in NH_4HF_2 containing electrolyte is better than that formed in KF containing

electrolyte. In general, the discharge sparks are finer and homogeneous in these two F-containing electrolytes. This phenomenon is tied to the refinement effect of F^- ions [26]. When $C_3H_8O_3$ was added into the base electrolyte which contained NH_4HF_2, the discharge sparks became larger and the electrolyte temperature was much higher, but the sparks in this electrolyte were still uniform during the entire MAO process. This is because $C_3H_8O_3$, as a kind of stabilizer, can effectively reduce the poor thermal effect produced by oxidation reaction of magnesium alloys. So $C_3H_8O_3$ is a good additive in the base electrolyte. On this basis, H_2O_2 was also added. The duration of spark discharge was prolonged and a sharp popping sound arose during the reaction. It was clear that a mass of bubbles generated during reactions between substrate and electrolyte, which was related to the decomposition of H_2O_2. Besides, point discharge phenomenon was observed in all electrolytes with different additives. This is because the energy of point area is easy to concentrate.

3.2. Appearance and thickness of coatings

The appearance of samples prior to immersion in 1.0 SBF is shown in Fig. 1. The color of surface coating of sample A2, A5, A9 and A11 are pale yellow, gray, yellow and white, respectively. The color of the coating varies with different additives. It can be explained by the influence of elements involved in MAO reaction by diffusion or electromigration effects on composition and structure of the coating. As shown in Fig. 1(a), there were some rough pits on the edge of the coating. KF is a kind of strong electrolyte which greatly improves the electrolyte conductivity. The nonuniform distribution of electric field leads to concentration of energy on the edge of the samples. Much more fused alloys are produced here, and then cold electrolyte brings about the rapid solidification of these fused alloys as well as superior structural stress. Fig. 2 gives the thickness of MAO coatings formed in base electrolyte with introduce of different additives. From A1 to A3, A4 to A6, A7 to A9 and A10 to A12. A tendency that the coating thickness increased with increasing concentration of one kind of additive alone in electrolyte was shown. However, there are few differences among thickness of all coating. It means that the improvement of coating thickness of additives is limited under otherwise equal conditions. Maximum thickness was found from the coating produced in the electrolyte with 7 g/L NH_4HF_2. The MAO process is characterized by a complex four-phase system (metal–dielectric–gas–electrolyte) with a number of possible phase boundaries. The formation and thickness of the coatings are related to the electrical conductivity of the complex four-phase system. Research results showed that the introduce of compounds containing F^- ion helped to increase the electrical conductivity of the electrolyte and was favorable to the formation of the MAO coatings [27]. The high viscosity of $C_3H_8O_3$ can hinder the migration of ions in electrolyte and then reduce the electrical conductivity of the whole system. The introduce of H_2O_2 can make gas libration much more intense and extend the period of time during which gas bubbles emerge, subsequently the anode surface is covered with a continuous gas envelope and the electrical conductivity of the four-phase system decreases. So the coating thickness decreases when $C_3H_8O_3$ or (and) H_2O_2 is (are) added to the electrolyte.

3.3. Phase structure

Fig. 3 is the XRD pattern of ZK60 magnesium alloy. Two kinds of phases, Mg and $MgZn_2$, are observed in the pattern. The XRD patterns of MAO coatings obtained in electrolyte

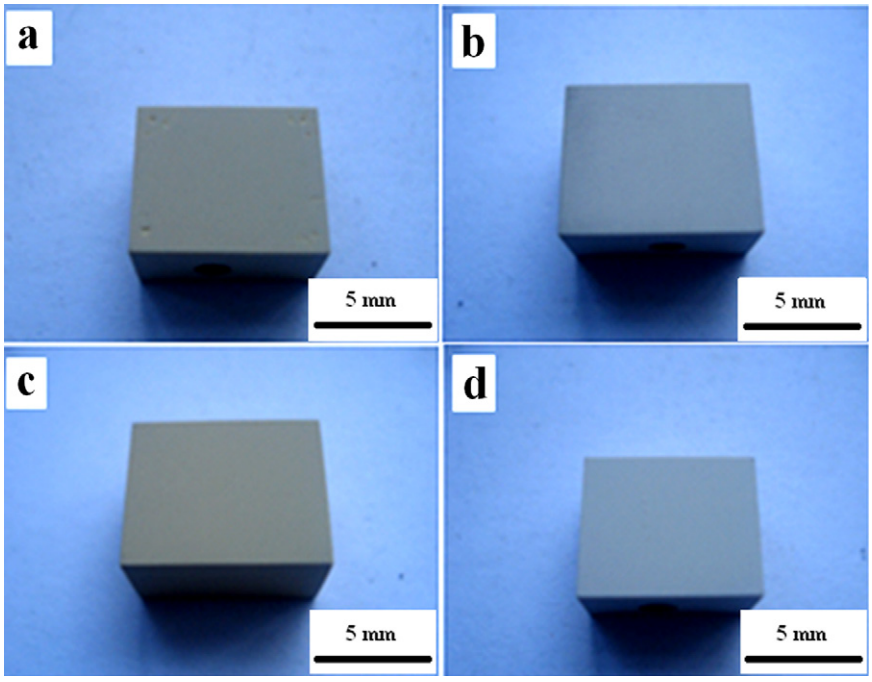

Fig. 1. Appearance of MAO sample: (a) A2, (b) A5, (c) A9, and (d) A11.

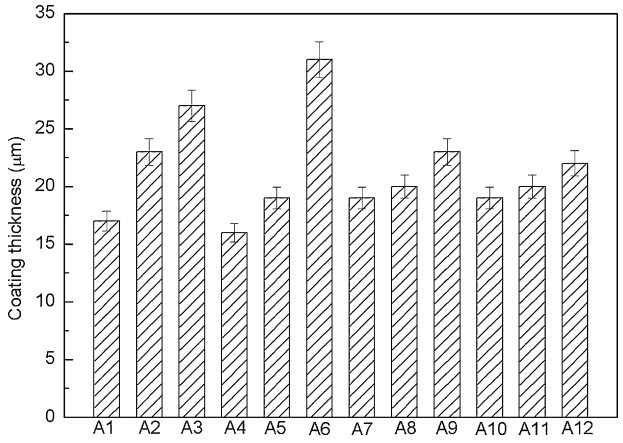

Fig. 2. Coatings thickness with respect to base electrolyte with introduce of different additives.

with different additives are shown in Fig. 4. It can be seen that these MAO coatings are mainly composed of Mg_2SiO_4, $MgSiO_3$ and SiO_2 in spite of different additives. The intensity of peaks corresponding to the magnesium phase of substrate is very strong, indicating that X-ray can easily penetrate the MAO coating because of the porous structure and thin thickness of the coatings. It is clear that the intensity of peaks corresponding to substrate of Fig. 4(a) is obviously stronger than that of the other three figures. It means that the coating formed in KF-containing electrolyte is much easier to be penetrated. But there are not many differences between their coating thicknesses. So it is likely that the coating formed in KF containing electrolyte is loose textured and contains many micropores inside. When H_2O_2 was added to the electrolyte, the diffraction peaks of MgO phase show in Fig. 4(d) clearly.

Owing to the instantaneous high temperature that can reach several thousand degrees in the microarc sparking zone, MgO forms by outward migration of Mg^{2+} and inward migration of O^{2-} as listed by the following reaction:

$$Mg^{2+} + O^{2-} \rightarrow MgO$$

There are two kinds of formation mechanism of SiO_2. Firstly, the incorporation of silicon during micriarc oxidation

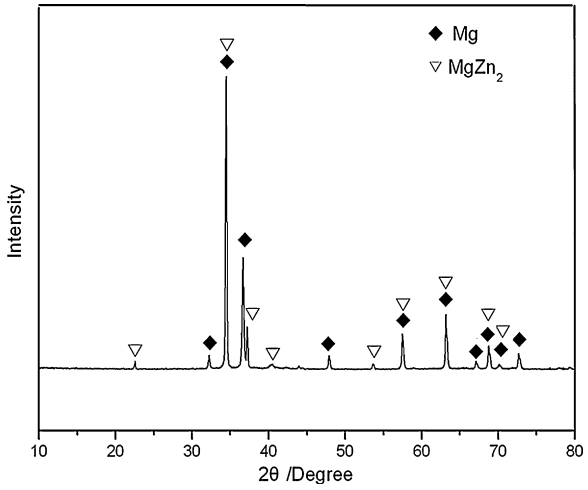

Fig. 3. XRD patterns of ZK60 magnesium alloy.

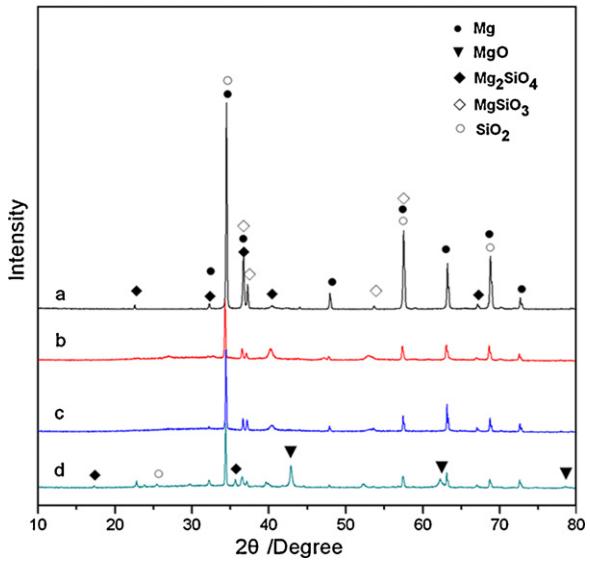

Fig. 4. XRD patterns of MAO coatings formed in the base electrolyte with different additives: (a) sample A3, (b) sample A6, (c) sample A7, and (d) sample A11.

likely arose by the deposition of colloidal silica. This may form by the acidification of the solution near the alloy surface, according to the following reactions [28]:

$$4H_2O \rightarrow 4H^+ + 4OH^-$$

$$SiO_4^{4-} + 4H^+ \rightarrow Si(OH)_4$$

$$Si(OH)_4 + Si(OH)_4 + \cdots \rightarrow (xSiO_2 \cdot yH_2O)$$

$$(xSiO_2 \cdot yH_2O) \rightarrow xSiO_2 + yH_2O$$

Another possible way for the formation of SiO_2 is shown in the following reaction [29]:

$$SiO_4^{4-} \rightarrow SiO_2 + O_2\uparrow + 4e^-$$

The formation of $MgSiO_3$ and Mg_2SiO_4 is due to a high temperature phase transformation between fused SiO_2 and MgO through the following reactions:

$$MgO + SiO_2 \rightarrow MgSiO_3$$

$$2MgO + SiO_2 \rightarrow Mg_2SiO_4$$

It is likely that the large amounts of oxygen released by decomposition of H_2O_2 hinder the reaction between SiO_2 and MgO and create favorable conditions for the healthy growth combination of outward Mg^{2+} and inward O^{2-}.

3.4. Surface and cross-section morphology

The surface and cross-section morphologies of ceramic coatings are shown in Fig. 5. It is seen that a porous network microstructure has been formed on the coating surface. There are protuberant areas, concave areas and particles around the pores. The micropores homogeneously distribute all over the coating surface. There are no cracks on the entire coatings

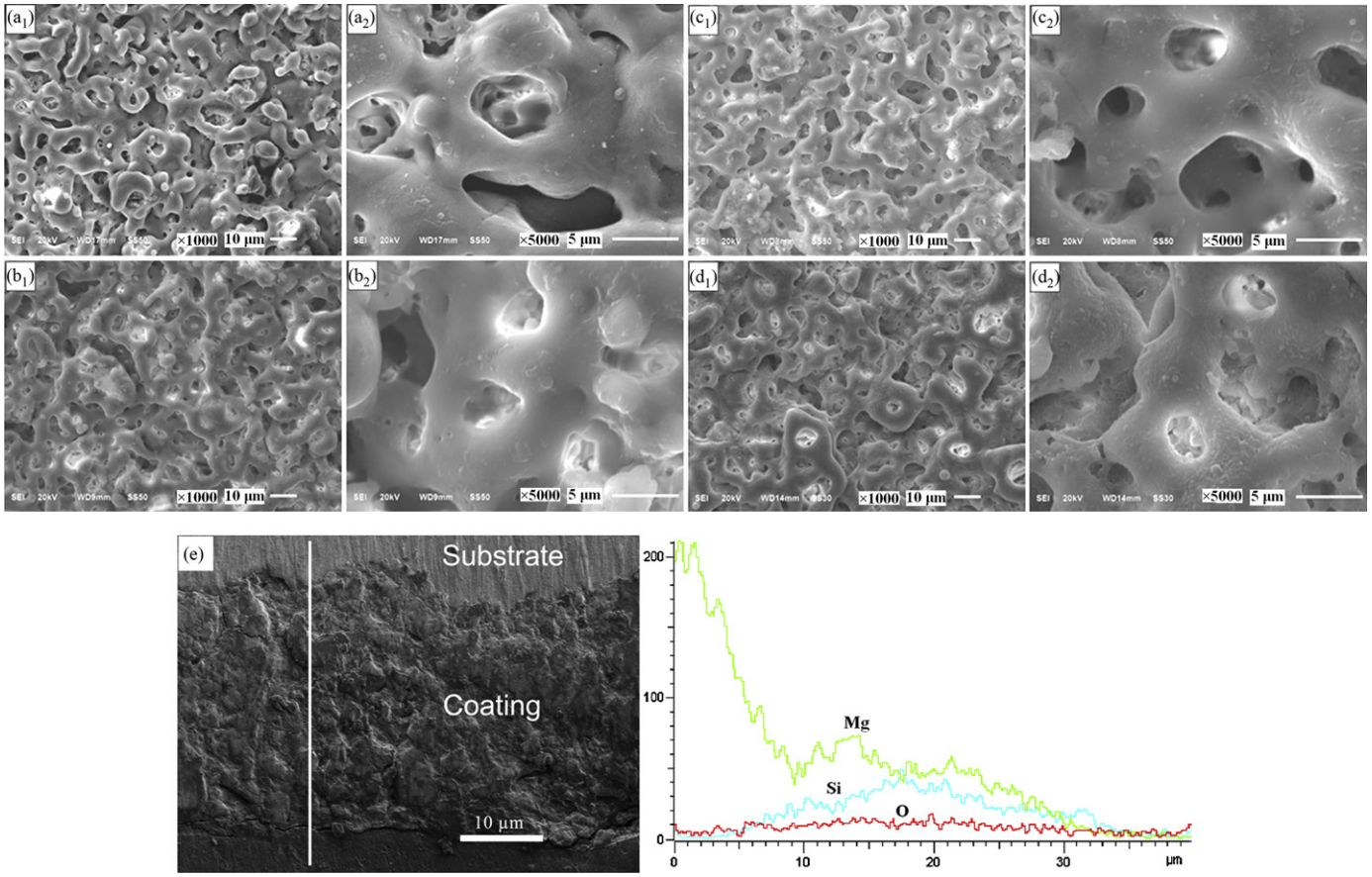

Fig. 5. SEM surface and cross-section morphologies of MAO coatings formed in the base electrolyte with different additives: (a) sample A3, (b) sample A6, (c) sample A7, (d) sample A11, (e) cross-section morphology and linear element distribution of sample A6.

surface. The micropores are formed by molten oxide and gas bubbles thrown out of microarc discharge channels and they are channels of micro-arc discharge in electrolyte [30]. During the MAO process, when the voltage increases to puncture voltage, high temperature arises instantly and accompanied by spark discharge phenomenon and then transparent passive coating formed beforehand on magnesium alloys surface is broken down, magnesium and alloying elements are melted out of the substrate. Because of the resistance difference of different parts of the samples, the weakest area is broken down preferentially. The compression produced during the oxidation treatment is responsible for the eruption of gas bubbles covered by the sintered material and the formation of pores on the coating surface. So the MAO coatings show a porous surface morphology.

Compared with Fig. 5(a), it can be seen that the introduce of NH_4HF_2 has a little effect on the change of coating surface morphologies in Fig. 5(b). From Fig. 5(c), the introduce of $C_3H_8O_3$ makes the coating denser and the pore size closer to each other. It is related to the stabilizing reaction and resisting point discharge effects of $C_3H_8O_3$. The coating surface became rough when H_2O_2 was added to the electrolyte. This is because the decomposition of H_2O_2 releases a large amount of oxygen and fused substrate erupts outwards accompanied by the gas under great pressure.

The cross-section SEM image and linear element distribution of ceramic coating fabricated on sample A6 is shown in Fig. 5(e). As shown in Fig. 5(e), the coating is about 32 μm and the coating contains elements of Mg, Si and O. It implies that the elements in electrolyte were incorporated into the coating through MAO reaction. There is no apparent discontinuity to the substrate in the bonding zone. It indicates that excellent metallurgical bonding occurs between the ceramic coating and the substrate. The inner layer of the coating is denser than the outmost layer. No pores but a crack is observed at the outmost

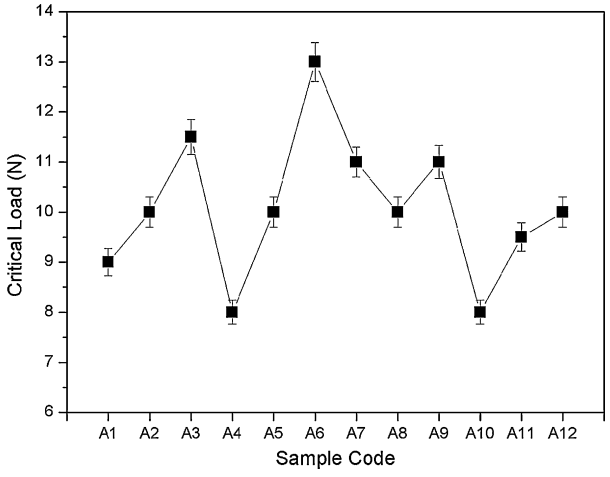

Fig. 6. The dependence of the critical load on different additives.

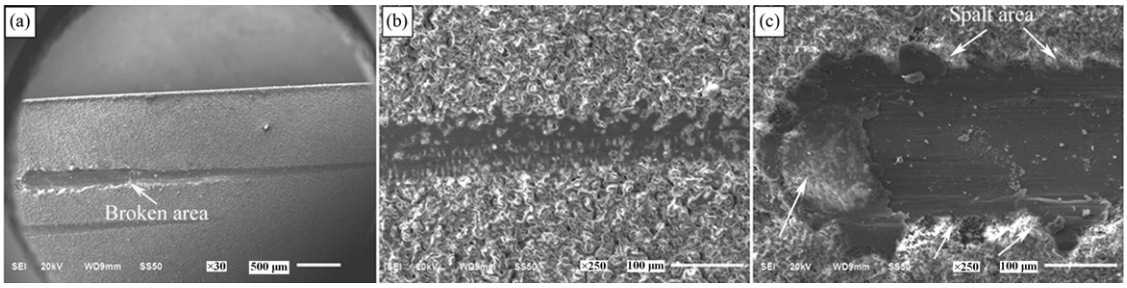

Fig. 7. SEM micrographs of scratch test of MAO coating formed in the base electrolyte with 7 g/L NH_4HF_2, 5 mL/L $C_3H_8O_3$, 15 mL/L H_2O_2: (a) is the whole scratch; (b) is the beginning of the scratch; (c) is the ending of the scratch.

Table 2
Weight loss of samples immersed in 1.0 SBF.

Sample code	0 d	3 d	5 d	7 d	9 d	Weight loss (g)	Weight loss percentage (%)
A1	1.2180	1.2184	1.1913	1.1826	1.1316	0.0872	7.12
A2	1.2248	1.2252	1.2024	1.1798	1.1446	0.0810	6.58
A3	1.2512	1.2516	1.2342	1.2005	1.1755	0.0765	6.08
A4	1.2719	1.2724	1.2480	1.2366	1.1182	0.1547	12.11
A5	1.3227	1.3230	1.2937	1.2827	1.2607	0.0626	4.71
A6	1.2804	1.2809	1.2632	1.2250	1.2340	0.0474	3.63
A7	1.2314	1.2317	1.2194	1.1823	1.1869	0.0451	2.07
A8	1.2129	1.2133	1.2000	1.1601	1.1683	0.0454	3.71
A9	1.2429	1.2434	1.2265	1.2496	1.1936	0.0503	4.01
A10	1.3195	1.3199	1.3025	1.2921	1.2374	0.0829	6.25
A11	1.2930	1.2935	1.2753	1.2642	1.2626	0.0314	2.39
A12	1.2937	1.2942	1.2758	1.2386	1.2333	0.0614	4.71

layer of the coating which may due to the loose and brittle structure of the outmost porous layer.

3.5. The coating adhesion

The dependence of the critical load on different additives is shown in Fig. 6. The highest adhesion value (13 N) is observed for the coating of sample A6. The coating adhesion increases with increasing concentration of one kind of additive alone in electrolyte, which has the same tendency with the coating thickness. The introduce of $C_3H_8O_3$ keeps the coating adhesion at a relatively high value while the introduce of H_2O_2 reduces the coating adhesion. This phenomenon can be explained by the combination of coating thickness and structure compactness.

Fig. 7 shows the SEM of scratch of MAO coating of sample A11. From Fig. 7(a), macroscopical morphology of the coating scratch can be seen. The ceramic coating was pressed to the two sides by indenter and then a scratch track was left. In Fig. 7(b), the micropores can still be seen clearly at the beginning of the scratch, as the extension of the scratch, the micropores structure becomes unconspicuous, when the coating is penetrated, i.e. reaching the upper critical load, substrate is exposed to the air (in Fig. 7(c)). There existed stratified spalling phenomenon in the spalt area of the scratch.

3.6. The coating corrosion resistance

The weight loss of samples immersed in 1.0 SBF is shown in Table 2. From the data listed in Table 2, the coating formed in the base electrolyte with introduce of 3 g/L NH_4HF_2 is corroded seriously and its corrosion resistance is the lowest of all coatings. Compared the weight loss percentages of coatings prepared in the base electrolyte with introduce of KF (sample A2 and A3), it is concluded that the corrosion resistance of coatings prepared in the base electrolyte with introduce of NH_4HF_2 (sample A5 and A6) is much better and the weight loss of immersed coating is the lowest when the concentration of NH_4HF_2 is 7 g/L. So the best adding concentration of NH_4HF_2 is 7 g/L. The same method is used to determine the best concentration of $C_3H_8O_3$. The best adding concentrations of $C_3H_8O_3$ is 5 mL/L. The ceramic coatings formed in base electrolyte containing 7 g/L NH_4HF_2 and 5 mL/L $C_3H_8O_3$ exhibit the highest corrosion resistance. The weight loss percentages of sample A10, A11and A12 are higher than that of sample A7, which infers that the introduce of H_2O_2 is unfavorable to the coating corrosion resistance. Because the masses of oxygen generated by the decomposition of H_2O_2 reduce the coating compactness and make the coating micropores bigger. The edge of the samples is corroded firstly. This is because electric field lines are concentrative on the edge of the samples during the MAO process and it is the reason for the weak ability of sharp corner and edge to resist SBF corrosion. In contrast, the surface of the sample is relatively anti-corrosive.

4. Conclusion

(1) The four kinds of additives (i.e. KF, NH_4HF_2, $C_3H_8O_3$ and H_2O_2) play different roles in the formation of MAO coatings. Both KF and NH_4HF_2 promote discharge and accelerate reaction. $C_3H_8O_3$ can effectively reduce the poor thermal effect produced by oxidation reaction of magnesium alloys as

stabilizer. The introduce of H_2O_2 results in oxygen libration and makes coating surface rough.

(2) The MAO coatings are mainly composed of Mg_2SiO_4, $MgSiO_3$ and SiO_2 in spite of different additives, but the intensity and width of diffraction peaks are variational. The introduce of H_2O_2 hinders the reaction between SiO_2 and MgO and creates favorable conditions for the formation of the MgO phase.

(3) The color of the coatings varies with different additives. Porous network microstructure is formed on the coating surface. The micropores homogeneously distribute all over the surface. There are no cracks on the entire surface of all coatings. The introduce of $C_3H_8O_3$ makes the coating denser and the pore size closer to each other.

(4) The coating formed in the base electrolyte with introduce of 3 g/L NH_4HF_2 is corroded seriously and its corrosion resistance is the lowest of all coatings. The ceramic coatings formed in base electrolyte containing 7 g/L NH_4HF_2 and 5 mL/L $C_3H_8O_3$ exhibit the highest corrosion resistance. The introduce of H_2O_2 reduces the coating compactness, makes the coating micropores bigger and decreases the coating corrosion resistance.

Acknowledgments

This work is part of a research program financed by Science and Technology Supporting System Item of Resource-conserving Society of Shandong Province (Project No. 2007JY05) and the Development Project of Science and Technology of Shandong Province (Project No. 2010GSF10627).

References

[1] J.E. Gray, B. Luan, Protective coatings on magnesium and its alloys—a critical review, Journal of Alloys and Compounds 336 (2002) 88–113.

[2] R.V. Subba Rao, U. Wolff, S. Baunack, J. Eckert, A. Gebert, Corrosion behaviour of the amorphous $Mg_{65}Y_{10}Cu_{15}Ag_{10}$ alloy, Corrosion Science 45 (2003) 817–832.

[3] S. Mathieu, C. Rapina, J. Hazanb, P. Steinmetza, Corrosion behavior of high pressure die-cast and semi-solid cast AZ91D alloys, Corrosion Science 44 (2002) 2737–2756.

[4] L. Wang, T. Shinohara, B.P. Zhang, Influence of chloride, sulfate and bicarbonate anions on the corrosion behavior of AZ31 magnesium alloy, Journal of Alloys and Compounds 496 (2010) 500–507.

[5] D. Nam, W.C. Kim, J.G. Kima, K.S. Shin, H.C. Jung, Corrosion resistance of Mg–5Al–*x*Sr alloys, Journal of Alloys and Compounds 509 (2011) 4839–4847.

[6] Y.J. Zhang, C.W. Yan, F.H. Wang, H.Y. Lou, C.N. Cao, Study on the environmentally friendly anodizing of AZ91D magnesium alloy, Surface and Coatings Technology 161 (2002) 36–43.

[7] A.K. Sharma, R. Uma Rani, A. Malek, K.S.N. Acharya, M. Muddu, S. Kumar, Black anodizing of a magnesium–lithium alloy, Metal Finishing 94 (1996) 16.

[8] K.Z. Chong, T.S. Shih, Conversion-coating treatment for magnesium alloys by a permanganate-phosphate solution, Materials Chemistry and Physics 80 (2003) 191–200.

[9] S. Kozerski, L. Pawlowski, R. Jaworski, F. Roudet, F. Petit, Two zones microstructure of suspension plasma sprayed hydroxyapatite coatings, Surface and Coatings Technology 204 (2010) 1380–1387.

[10] X. Lu, Z.F. Zhao, Y. Leng, Two zones microstructure of suspension plasma sprayed hydroxyapatite coatings, Surface and Coatings Technology 27 (2007) 700–708.

[11] C.Y. Zhang, R.C. Zeng, R.S. Chen, C.L. Liu, J.C. Gao, Preparation of calcium phosphate coatings on Mg–1.0Ca alloy, Transactions of Nonferrous Metals Society of China 20 (2010) S655–S659.

[12] Y.W. Song, D.Y. Shan, E.H. Han, Electrodeposition of hydroxyapatite coating on AZ91D magnesium alloy for biomaterial application, Materials Letters 62 (2008) 3272–3279.

[13] H.F. Guo, M.Z. An, Growth of ceramic coatings on AZ91D magnesium alloys by micro-arc oxidation in aluminate-fluoride solutions and evaluation of corrosion resistance, Applied Surface Science 246 (2005) 229–238.

[14] Y. Ma, X. Nie, D.O. Northwood, H. Hu, Corrosion and erosion properties of silicate and phosphate coatings on magnesium, Thin Solid Films 469–470 (2004) 472–477.

[15] A.L. Yerokhin, A. Shatrov, V. Samsonov, P. Shashkov, A. Leyland, A. Matthews, Fatigue properties of Keronite coatings on a magnesium alloy, Surface and Coatings Technology 182 (2004) 78–84.

[16] L.O. Snizhko, A.L. Yerokhin, A. Pilkington, N.L. Gurevina, D.O. Misnyankin, A. Leyland, A. Matthews, Anodic processes in plasma electrolytic oxidation of aluminium in alkaline solutions, Electrochimica Acta 49 (2004) 2085–2095.

[17] X. Nie, A. Leyland, A. Matthews, Deposition of layered bioceramic hydroxyapatite/TiO_2 coatings on titanium alloys using a hybrid technique of micro-arc oxidation and electrophoresis, Surface and Coatings Technology 125 (2000) 407–414.

[18] X.J. Li, G.A. Cheng, W.B. Xue, R.T. Zheng, Y.J. Cheng, Wear and corrosion resistant coatings formed by microarc oxidation on TiAl alloy, Materials Chemistry and Physics 107 (2008) 148–152.

[19] Y.K. Shin, W.S. Chae, Y.W. Song, Y.M. Sung, Formation of titania photocatalyst films by microarc oxidation of Ti and Ti–6Al–4V alloys, Electrochemistry Communications 8 (2006) 465–470.

[20] S. Verdier, M. Boinet, S. Maximovitch, F. Dalard, Formation, structure and composition of anodic films on AM60 magnesium alloy obtained by DC plasma anodising, Corrosion Science 47 (2005) 1429–1444.

[21] Y.M. Wang, D.C. Jia, L.X. Guo, T.Q. Lei, B.L. Jiang, Effect of discharge pulsating on microarc oxidation coatings formed on Ti6Al4V alloy, Materials Chemistry and Physics 90 (2005) 128–133.

[22] V.S. Rudnev, T.P. Yarovaya, D.L. Boguta, L.M. Tyrina, P.M. Nedozorov, P.S. Gordienko, Anodic spark deposition of P, Me(I1) or Me(II1) containing coatings on aluminium and titanium alloys in electrolytes with polyphosphate complexes, Journal of Electroanalytical Chemistry 497 (2001) 150–158.

[23] D. Wu, X.D. Liu, K. Lu, Y.P. Zhang, H. Wang, Influence of $C_3H_8O_3$ in the electrolyte on characteristics and corrosion resistance of the microarc oxidation coatings formed on AZ91D magnesium alloy surface, Applied Surface Science 255 (2009) 7115–7120.

[24] A. Sabooria, M. Rabieea, F. Moztarzadeha, M. Sheikhib, M. Tahriria, M. Karimi, Synthesis, characterization and in vitro bioactivity of sol-gel-derived SiO_2–CaO–P_2O_5–MgO bioglass, Materials Science and Engineering C 29 (2009) 335–340.

[25] T. Kokubo, H. Kushitani, S. Sakka, T. Kitsugi, T. Yamamuro, Solutions able to reproduce in vivo surface-structure changes in bioactive glass-ceramics A-W, Journal of Biomedical Materials Research 24 (1990) 721–734.

[26] J. Liang, B. Guo, J. Tian, H.W. Liu, J.F. Zhou, T. Xu, Effect of potassium fluoride in electrolytic solution on the structure and properties of microarc oxidation coatings on magnesium alloy, Applied Surface Science 252 (2005) 345–351.

[27] A.L. Yerokhin, X. Nie, A. Leyland, A. Matthews, S.J. Dowey, Plasma electrolysis for surface engineering, Surface and Coatings Technology 122 (1999) 73–93.

[28] V. Brass, S. Xia, R. Yue, G. Richard, Rateick Jr., Characterization of oxide films formed on Mg-based WE43 alloy using AC/DC anodization in silicate solutions, Journal of the Electrochemical Society 151 (2004) B1–B10.

[29] O. Khaselev, D. Weiss, J. Yahalom, Anodizing of pure magnesium in KOH-aluminate solutions under sparking, Journal of the Electrochemical Society 146 (1999) 1757–1761.

[30] G.Y. Liu, J. Hu, Z.K. Ding, C. Wang, Bioactive calcium phosphate coating formed on micro-arc oxidized magnesium by chemical deposition, Applied Surface Science 257 (2011) 2051–2057.